Detecting intense hurricanes from low resolution datasets via dynamical indicators

Davide Faranda, Gabriele Messori, Pascal Yiou, Soulivanh Thao, Flavio Pons, Berengere Dubrulle

Detecting intense hurricanes from low resolution datasets via dynamical indicators

Davide Faranda*

Laboratoire des Sciences du Climat et de l'Environnement, CEA Saclay l'Orme des Merisiers, UMR 8212 CEA-CNRS-UVSQ, Université Paris-Saclay & IPSL, 91191, Gif-sur-Yvette, France; London Mathematical Laboratory, 8 Margravine Gardens, London, W6 8RH, UK; LMD/IPSL, Ecole Normale Superieure, PSL research University, 75005, Paris, France

Gabriele Messori

Department of Earth Sciences, Uppsala University, and Centre of Natural Hazards and Disaster Science (CNDS), Uppsala, Sweden; Department of Meteorology, Stockholm University, and Bolin Centre for Climate Research,Stockholm, Sweden.

Pascal Yiou, Soulivanh Thao, Flavio Pons

Laboratoire des Sciences du Climat et de l'Environnement, CEA Saclay l'Orme des Merisiers, UMR 8212 CEA-CNRS-UVSQ, Université Paris-Saclay & IPSL, 91191, Gif-sur-Yvette, France

Berengere Dubrulle

SPEC, CEA, CNRS, Université Paris-Saclay, F-91191 CEA Saclay, Gif-sur-Yvette, France

*Corresponding author address: Davide Faranda, Laboratoire des Sciences du Climat et de l'Environnement, CEA Saclay l'Orme des Merisiers, UMR 8212 CEA-CNRS-UVSQ, Université Paris-Saclay & IPSL, 91191, Gif-sur-Yvette, France

E-mail: davide.faranda@lsce.ipsl.fr

ABSTRACT

Although the life-cycle of hurricanes is well understood, many of the underlying physical processes occur at scales below those resolved by global climate models (GCMs), so that projecting future changes in hurricance characteristics remains challenging. We assess the capability of dynamical system metrics to identify intense cyclones even in coarse resolution datasets, where wind speed may be not accurately represented. We compute dynamical indicators, namely the persistence and number of active degrees of freedom, from the horizontal wind field of 146 tropical cyclones occurred between 2010 and 2018 using ERA5 reanalysis data at 0.25 $^{\circ}$ horizontal resolution, and link these to the maximum sustained winds as detected from observational datasets. Our analysis provides a representation of cyclones in phase space and allows to: i) identify different stages of the cyclones' life cycle as distinct regions of the phase space; and ii) locate regions of the phase space associated with intense cyclones (as detected from observations). Specifically, we find that the most intense cyclones are associated with a strong decrease of the instantaneous dimension and an increase in persistence of tropical cyclones. This relation could be used for detection of intense cyclones in comparatively coarse resolution datasets, such as those issued from GCM simulations or century-long reanalyses.

1. Introduction

Tropical cyclones are high-impact extreme weather events. In the United States of America, they are the costliest natural disaster category (Smith and Katz 2013; Grinsted et al. 2019), with the damage related to hurricane Katrina (2005) alone amounting to about 1% of the country's gross domestic product (Grinsted et al. 2019). Trends in the frequency of occurrence or intensity of tropical cyclones are difficult to discern in observations, because of the comparative rarity of the events and of the brevity of highly spatially and temporally resolved datasets, which rely on in-situ and satellite observations (Chang and Guo 2007). Projections of future climate indicate an increase in the intensity of hurricanes in the North Atlantic sector, albeit only with medium confidence (Kossin et al. 2017) because of the difficulties in reproducing the dynamics of the most severe hurricanes even in the most advanced global or regional climate models (Roberts et al. 2020b). Indeed, while mid-latitudes synoptic dynamics mostly originates from the chaotic structure of the motions associated with baroclinic instability (Lorenz 1990; Schubert and Lucarini 2015), tropical cyclones are characterized by a rapid organization of convectively unstable flows whose dynamics is turbulent and highly sensitive to boundary conditions (Muller and Romps 2018).

Destructive tropical cyclones often experience rapid intensification, which occurs when a tropical cyclone gains dramatically in strength over a short period of time (Sanders 1986). The rapid intensification phenomenon, well explained from a theoretical viewpoint (Klein 2010; Soloviev et al. 2017), results in an enhancement of the destructive potential of the cyclone and in a degraded predictability of its trajectory (Lee et al. 2016). It is often detected via an increment(generally 40 Kts) of sustained winds over a period of 24h. It is challenging to detect this phenomenon in global climate models (GCMs), due to the coarse resolution of wind field data. Emanuel (2017) discusses

several wide-reaching implications of the poor representation of hurricanes in GCMs for present and future climates.

Here, we investigate whether it may be possible to obtain a reliable indicator of intense tropical cyclones from relatively coarse gridded atmospheric data. Specifically, we compute two metrics that describe cyclones as states of a chaotic high-dimensional dynamical system, and reflect the persistence and dimension (i.e. the number of active degrees of freedom) of instantaneous states of the cyclones. These metrics have recently provided insights on a number of geophysical phenomena, including transitions between transient metastable states of the mid-latitude atmosphere (Faranda et al. 2017; Hochman et al. 2019), palaeoclimate attractors (Brunetti et al. 2019; Messori and Faranda 2021) slow earthquake dynamics (Gualandi et al. 2020) and changes in mid-latitude atmospheric predictability under global warming (Faranda et al. 2019). All these applications have taken a Eulerian approach, and have thus focused on a fixed spatio-temporal domain, rather than tracking the evolution of specific physical phenomena. Here, we apply for the first time the two metrics in a Lagrangian perspective. A Lagrangian dynamical systems framework is particularly convenient to study the complex behavior of convectively unstable flow systems (Crisanti et al. 1991; Vulpiani 2010), such as tropical convection. As an additional benefit over previous dynamical systems approaches (e.g Wolf et al. 1985; Cao 1997), these metrics can be easily applied to large datasets, such as climate reanalyses or climate models. Their Lagrangian implementation enables to characterize the phase-space structure of tropical cyclones in terms of their dimension and persistence, and observe whether these single out the most intense cyclones. The rationale is that the signature of intense cyclones propagates through scales due to the presence of inverse cascades as suggested by Levich and Tzvetkov (1985) and, more recently, by Faranda et al. (2018). If this were indeed the case, we could then use the region of phase space targeted by intense cyclones in observations to detect the same phenomenon in datasets where we cannot explicitly access the

relevant spatial scales. Our study is organized as follows: first, we describe the data, observables for cyclone dynamics and the theoretical bases supporting the computation of the dynamical indicators. Then, we show the general characteristics of the phase space of tropical cyclones for the different observables. Finally, we investigate rapid intensification and discuss our results.

2. Data and Methods

a. Representation of tropical cyclones in ERA5 data

We follow 146 Atlantic tropical cyclones which occurred between 2010 and 2018 and base the computation of the two dynamical systems metrics on hourly-mean data from the ERA5 reanalysis (Hersbach et al. 2020) sampled every 6h, and additionally whenever the HURDAT2 database (Landsea and Franklin 2013) displays a cyclone landfall entry. Tracks and classification of the cyclones are also taken from the HURDAT2 database (Landsea and Franklin 2013). HURDAT2 is the most complete database of tropical cyclone tracks for the Atlantic basin since 1950, providing 6-hourly sampling of position and speed of the eye, and maximum sustained winds at a 5 kts resolution. No wind speed adjustment has been made, contrary to what is done by Emanuel et al. (2005).

There is a large discrepancy between the maximum sustained winds reported in HURDAT2 and the closest quantity that we can derive from ERA5, namely the maximum horizontal wind at 1000 hPa over one hour, shown in Figure 1. It is important to remark that, while ERA5 wind speed is averaged over one hour, tropical cyclone intensity is usually defined using the one-minute average. This reflects on the large discrepancy between the highest wind values found in ERA5 ($\approx$ 80 kts) and in HURDAT2 ($\approx$ 150 kts). This affects the capability of ERA5 to both accurately assign each hurricane to the appropriate Saffir-Simpson category and to detect rapid intensification. In

particular, for cyclone intensity estimation, this implies that we are not able to separate hurricanes between category 2 and 5. Concerning rapid intensification, HURDAT2 points to 47 out of the 146 considered cyclones, while ERA5 detects none. This analysis suggests that ERA5 shares the difficulties of current state-of-the-art GCMs when it comes to representing the intensity of tropical cyclones Kim et al. (2018). We also underline that the ERA5 horizontal resolution used here is of the same order of magnitude as that of the HighResMIP (High Resolution Model Intercomparison Project, Haarsma et al. (2016)) and PRIMAVERA models, which are amongst the current best tools to study climate change impacts on tropical cyclones (Roberts et al. 2020a).

b. Observables of cyclone dynamics

We adopt a Lagrangian framework, i.e. we consider a domain of size $\sim$ 1200 km $\times$ 1200 km (41×41 grid points), centred on the eye of each cyclone. In the vertical dimension, we consider 9 pressure levels from 1000 hPa to 200 hPa. As observables, we chose sea-level pressure (SLP) maps, horizontal velocity at 1000 hPa (VH), vertical velocity (W) and the 3D kinetic energy field computed at each grid point as half of the quadratic sum of the velocity components. We relate these quantities to the maximum sustained winds derived from the HURDAT2 database, a quantity that can be directly connected to the economic loss caused by tropical cyclones (Zhai and Jiang 2014).

c. A dynamical systems view of tropical cyclones

We follow tropical cyclones in phase space as states of a chaotic high-dimensional dynamical system. Each instantaneous state of the cyclone, as represented by a given atmospheric variable, corresponds to a point along the trajectory representing the evolution of the system, which we sample at discrete intervals determined by the temporal resolution of our data. For example, we

may have 6-hourly SLP latitude-longitude maps which, at every time step, are centred on the cyclone's eye. Our aim is to diagnose the dynamical properties of the instantaneous (in time) and local (in phase-space) states of the cyclone, as represented by the chosen atmospheric variable and chosen geographical domain (physical space in Fig. 2). To do so, we leverage two metrics issuing from the combination of extreme value theory with Poincaré recurrences (Freitas et al. 2010; Lucarini et al. 2012, 2016)

We first consider a long trajectory $x(t)$, which in our example would be given by $x =$SLP maps of all time steps for all tropical cyclones in our dataset, always centred on their eye. We thus effectively construct a Lagrangian observable. We further consider a state of interest ζ_x, which would correspond to a single SLP map drawn from this dataset (state ζ in Fig. 2). We then define logarithmic returns as:

$$g(x(t), \zeta_x) = -\log[\text{dist}(x(t), \zeta_x)] \tag{1}$$

Here, *dist* is the Euclidean distance between two SLP maps, but it can be any distance function between two vectors which tends to zero as the two vectors increasingly resemble each other. We thus obtain a time series of logarithmic returns g, which takes large values at times when x closely resembles ζ_x.

We next define exceedances as $u(\zeta_x) = \{t, g(x(t), \zeta_x) > s(q, \zeta_x)\}$, where $s(q, \zeta_x)$ is a high threshold corresponding to the qth quantile of $g(x(t), \zeta_x)$. These are effectively the previously-mentioned Poincaré recurrences, for the chosen state ζ_x (phase space in Fig. 2). The Freitas-Freitas-Todd theorem (Freitas et al. 2010; Lucarini et al. 2012) states that the cumulative probability distribution $F(u, \zeta)$ converges to the exponential member of the Generalised Pareto Distribution. We thus have that:

$$F(u,\zeta_x) \simeq \exp\left[-\vartheta(\zeta_x)\frac{u(\zeta_x)}{\sigma(\zeta_x)}\right] \tag{2}$$

The parameters u and σ depend on the chosen state ζ_x, while ϑ is the so-called extremal index, namely a measure of clustering of points near ζ_x (Moloney et al. 2019). We estimate it here using the Süveges Estimator (Süveges 2007).

From the above, we can define two dynamical systems metrics: local dimension (d) and persistence (θ^{-1}). The local dimension is given by $d(\zeta_x) = 1/\sigma(\zeta_x)$, with $0 < d < +\infty$. The persistence by $\theta^{-1}(\zeta_x) = \Delta t/\vartheta(\zeta_x)$, where Δt is the time step of the data being analysed and $0 \leq \theta \leq 1$.

While the derivation of d and θ^{-1} may seem very abstract, the two metrics can be related intuitively to the physical properties of the tropical cyclones. d is a proxy for the active number of degrees of freedom of the cyclones' instantaneous states, while θ^{-1} measures the persistence of such states.

3. Dynamical properties of tropical cyclones and their connection to sustained winds

We now turn to analysing the properties of tropical cyclones in phase space for the different observables described in Sect. 2 against the maximum sustained winds. We begin with SLP and KE. SLP is widely used in cyclone tracking (Elsner 2003), and provides a first approximation of the horizontal velocity stream function. KE is relevant to the study of cyclones because of both its direct connection with the wind speed and its link with the phases of rapid intensification/decay of the cyclones (Krishnamurti et al. 2005).

Figure 3 shows the values of dimension d and inverse persistence θ for SLP (a) and KE (b) against the maximum sustained wind. The values of d are bounded by $d < 35$ for both the observables, despite the kinetic energy being derived from the 3D wind field, while SLP is 2D. The range of local dimensions found is relatively low compared to the number of grid-points used, which is

order of 1600 for SLP and 16000 for KE. This means that the majority of the degrees of freedom are frozen when we follow coherent convective phenomena such as tropical cyclones. Moreover, although the range of values spanned by the local dimensions is similar for KE and SLP, the lag-0 correlation coefficient between d_{SLP} and d_{KE} is relatively low, at 0.2. The persistence range is different for SLP and KE, with $0.1 < \theta_{SLP} < 1$ and $0.1 < \theta_{KE} < 0.6$. If we convert these values to hours, we get that the SLP persistence range is between 1 and 10 hours and the KE persistence ranges between 2 and 10 hours. Despite the different range of values, the lag-0 correlation between θ_{SLP} and θ_{KE} is 0.4, higher than for d, suggesting that the two carry more mutual information.

Maximum sustained winds are closely connected to the values of d and θ for SLP and KE. For SLP (Figure 3a) we note a strong dependence of θ on the maximum sustained winds. Low-to-moderate winds are associated with non-persistent states of the cyclones, while stronger winds typically point to more persistent states. High but not extreme wind speed values (60 to 85 kts) are concentrated on particularly low values of θ_{SLP}. For large values of d_{SLP}, maximum sustained winds are typically weak. An even clearer relation emerges between d_{KE}, θ_{KE} and the maximum sustained winds (Figure 3b). There, the strongest winds are associated with the lowest values of d and θ.

Fig. 3c,d) shows the distributions of d and θ conditional on the HURDAT2 classification of the cyclones; the least organised states (tropical storms, blue) are characterised by low persistence and relatively high dimension. On the opposite end, low dimensional and highly persistent states correspond to Hurricanes (red) or extratropical transitions of tropical cyclones (black). As a caveat, we note that the most intense events somewhat deviate from the modal shifts between the distributions. For example, the d_{KE} distribution for Tropical Storms (blue line in the lower panel of Fig. 3d) shows a much higher mode than that for Hurricanes (red line).

We test for significant differences in storm dynamics separately for d_{SLP}, d_{KE}, θ_{SLP} and θ_{KE} by comparing the three densities for the cases of tropical storms, hurricanes, and extratropical transitions under the null hypothesis that they have the same distribution (side and bottom panels of 3c,d)). We choose the significance level $\alpha = 0.05$. In particular, we apply a Kruskall-Wallis test to determine if there are significant differences in location and a k-sample Anderson-Darling test for more general shape differences among the three distributions. Then, we perform pairwise Wilcoxon signed rank tests to determine which distribution is stochastically dominant compared to the others. Finally, we also repeat the Anderson-Darling test in a pairwise fashion to determine if there are differences in scale between distributions that do not show significant location shifts. All the grouped Anderson-Darling and Kruskall-Wallis tests reject H_0 (all p-values $< 2.2 \times 10^{-16}$), suggesting that at least one distribution is significantly different from the others in all cases, possibly due to a location shift. The pairwise Wilcoxon tests suggest that both d_{SLP} and d_{KE} for tropical storms are larger than for hurricanes and extratropical transitioning storms; moreover, d_{KE} for hurricanes is also larger than for extratropical storms. The pairwise Anderson-Darling test points to a difference in scale between hurricanes and extratropical storms even in d_{SLP}. All tests are significant for θ, showing the lowest persistence in the tropical storm stage and the highest during extratropical transitions (see Table 1).

Figure 4 shows the same analysis as in Figure 3 but for VH and W. VH is the closest quantity to the maximum sustained winds and W may be related to convection. d_{VH} and θ_{VH} show a strong dependence on the maximum sustained winds (Fig. 4a), with the extreme values all located in correspondence of minima of the dynamical indicators. For W, the distribution of θ exhibits two modes, resulting in the partial separation of two clouds of points in the in d-θ scatterplot (Fig. 4b). The largest sustained winds are found in correspondence with the d and θ minima of the cluster corresponding to larger θ. The analysis conditioned to different phases of the cyclones (Figure 4

c,d) shows that VH is possibly the observable that separates most clearly hurricanes from tropical storms, as the modes are distinct in both d_{VH} and θ_{VH}, whereas for W the separation is less evident.

As for Figure 3 we have tested the statistical significance of the differences among the distributions of d_{VH}, d_W, θ_{VH} and θ_W. The grouped Anderson-Darling and Kruskall-Wallis tests reject H_0 at all levels (all p-values $< 2.2 \times 10^{-16}$), suggesting at least one distribution being significantly different from the others. The pairwise Wilcoxon tests (Table 1) suggest that d_{VH} is shifted towards significantly larger values for tropical storms than for hurricanes, while d_W is centered around lower values for hurricanes. However, while the distributions of d_W for hurricanes and extratropical storms do not differ significantly in terms of location shift, the distribution of d_W for tropical storms is stochastically dominant respect to the case of extratropical storms, despite a visually small difference in the figure. Similar results hold for the persistence: θ_{VH} displays significantly larger values for tropical storms, while the distributions of hurricanes and extratropical storms are not statistically different. In the case of θ_W, the distribution for the hurricanes is shifted towards significantly lower values, while no difference is found between tropical and extratropical storms.

We remark that the dynamical systems indicators obtained using 1000 hPa horizontal velocity (Figure 3, panel c) provide the best separation between TS and HU/EX storms, with higher velocity values concentrated at low values of both indicators. We parameterize the relationship between maximum sustained wind v_{max} and d_{VH}, θ_{VH} with a multiple linear regression $v_{max,i} = \alpha + \beta_d d_{VH,i} + \beta_\theta \theta_{VH,i} + \varepsilon_i$, where i denotes the observation and ε_i is a Gaussian white noise sequence. Both dynamical systems indicators have a significant explanatory effect on v_{max} (p-values $< 3 \times 10^{-16}$), with $\beta_d = -1.14$, and $\beta_\theta = -72.16$. The persistence coefficient is two orders of magnitude larger (in absolute value) than the one of the dimension, despite there being only roughly one order of magnitude difference in the scales of the two variables, pointing

to a larger effect of θ_{VH}. The goodness of fit is $R^2 = 0.22$. This indicates that a large fraction of v_{max} variability cannot be explained by the two indicators alone, and/or the presence of strong nonlinearities that are not caught by linear regression.

In the dynamical systems framework, a collapse of degrees of freedom and an increase of persistence are indicative of approaching unstable fixed points, i.e. special states of the dynamics where temporal and spatial scales are deformed. An example is the behavior encountered in the Lorenz 1963 attractor (Lorenz 1963) near the unstable fixed points corresponding to the centres of the wings of the butterfly-shaped attractor, where both d and θ attain low values [Figure A1 in Faranda et al. (2017)]. We discuss the implications of this result for the numerical modelling of tropical cyclones in Sect. 6.

4. Dynamical Indicators and Rapid intensification

In the previous section, we have established that the dynamical indicators provide a clear separation of the different meteorological phases of tropical cyclones. Now we focus on the analysis on the transitions from tropical storms (TS) to hurricanes (HU). Our goal is to understand whether we can use the dynamical indicators to discriminate the transitions associated with rapidly intensifying cyclones from the others, and whether the dimension and persistence analysis could be used to detect rapid intensification in a statistical sense in coarse-resolution climate datasets. Rapid intensification is usually quantified using the increment Δv of maximum sustained winds over 24h. Several numerical thresholds to define rapid intensification exist (Knaff et al. 2020). Here, we use thresholds of $\Delta v >$50 Kts or $\Delta v >$ 40 Kts, namely the highest thresholds proposed by (Knaff et al. 2020).

In phase space, rapid changes of the dynamics correspond to transitions through different basins of the attractor (Ghil et al. 2008; Dijkstra 2013). The variation of the dynamical systems indicators

can track these transitions because of their direct connection with the underlying entropy of the system: the local dimension d is an instantaneous measure of the active degrees of freedom, and the persistence θ is related to the dominant time scale of the dynamics, i.e. the Lyapunov exponent (Faranda and Vaienti 2018). Both these quantities are known to be connected to the dynamical (Kolmogorov-Sinai) entropy, since the seminal work of Young (1982).

Results relating the dynamical system metrics to rapid intensification are presented in Figure 5, for the four observables used in this study: SLP (a), KE (b), VH (c) and W (d). Median values are represented by magenta stars (40 KtS) and crosses (50 KtS); ellipses represent one standard deviation from the median. Blue (red) large circles represent the median d for all tropical storms (hurricanes). The green crosses (ellipses) represent the median (standard deviation) of the values of the dimension and persistence for all the tropical storm to hurricane transitions. The results show that transitions associated to rapid intensification target a special region of the d, θ space for KE and for VH. They correspond to lower-dimensional and higher-persistence phases of the dynamics of the cyclones.

The decrease in local dimension and inverse persistence implies a decrease of the dynamical (Kolmogorov-Sinai (Young 1982; Latora and Baranger 1999)) entropy of the cyclones, namely a reduction of the kinetic degrees of freedom, as discussed in the previous section. Specifically, the Kolmogorov-Sinai entropy is linked to the Lyapunov exponents (van Beijeren and Dorfman 1995), whose number of positive values is related to d and whose leading value is linked to θ (Faranda and Vaienti 2018). It is counterintuitive that large dissipating systems such as rapidly intensifying cyclones yield low entropy states. However, one can observe that the tendency to the order in the dynamical entropy is balanced by enhanced thermodynamic entropy leading to convection and diabatic phenomena.

Finally, we remark that the relationship between rapid intensification and decrease in d_{KE}, d_{VH} and θ_{KE}, θ_{VH} is not systematic: the number of cyclones visiting the magenta balls in Figure 5 is larger than those experiencing rapid intensification, i.e. one cannot use the values of d and θ to identify in a deterministic sense cases of rapid intensification.

5. Implications of the results for the numerical simulation of tropical cyclones

The computation of the dynamical systems indicators for tropical cyclones has shown that there is a strong relationship between such indicators computed for coarse atmospheric fields and the maximum sustained winds taken from observations. In the most intense phase of the cyclones, large maximum sustained winds are associated to low values of both d and θ, in particular if these are estimated on the horizontal velocity field. From a dynamical system viewpoint, the explanation is that air parcels behave almost identically, with rotational degrees of freedom oriented along the global axis of the storm. This behavior is symptomatic of highly persistent, low-dimensional states found at unstable fixed points of the dynamics. These results imply that intense cyclones are characterized by different dynamical properties (entropy, stability) from those not accompanied by large maximum sustained winds and that d and θ give a very good degree of discrimination from the other, less intense, tropical cyclones. Similarly, transitions from tropical storms to hurricanes of rapidly intensifying cyclones primarily reside in particular regions of the d, θ space. This is particularly evident for the metrics computed on horizontal velocity (VH), but to a good degree also on 3D kinetic energy (KE). Vertical velocity (W) provides a less-clear separation, likely because, while the horizontal wind is driven by the cyclone structure and dynamics, the vertical velocities are linked to smaller structures such as convective cells not directly resolved in ERA5.

These theoretical considerations have a number of concrete implications for current research on hurricanes. Current GCMs — and even reanalysis products — struggle in reproducing maximum

sustained winds comparable to those observed (see Fig. 1). Our study offers a way of mapping intense cyclones in d, θ space and measure, in climate change model experiments or century-long reanalysis products, shifts towards smaller or larger values of the dynamical indicators. This, in turn, may provide a strategy for studying changes in hurricane intensity driven by anthropogenic forcing. Indeed, while d and θ may not be used to provide a deterministic indication of cyclone intensification, they do provide a robust statistical indication. Furthermore, the fact that the dynamics of intense hurricanes approaches that of fixed points of high-dimensional dynamical systems may explain why it is so difficult to adequately represent rapidly intensifying tropical cyclones and hurricanes in numerical models. Parameterizations are devised for typical states of tropical dynamics (disorganized storms) but not specifically for the organized states of tropical cyclones. As a caveat, we underline that our Lagrangian approach does not allow to relate the present results to the predictability of the trajectories of the tropical cyclones, unlike the Eulerian approach applied to extratropical motions in (Faranda et al. 2017; Messori et al. 2017).

Acknowledgments. This study is supported by the INSU CNRS LEFE-MANU grant DINCLIC and the ANR-TERC BOREAS . G. Messori was partly supported by the Swedish Research Council Vetenskapsrådet (grant no. 2016-03724). B. Dubrulle was partly supported by the ANR, project EXPLOIT, grant agreement no. ANR-16-CE06-0006-01.

References

Brunetti, M., J. Kasparian, and C. Vérard, 2019: Co-existing climate attractors in a coupled aqua-planet. *Climate Dynamics*, **53 (9-10)**, 6293–6308.

Cao, L., 1997: Practical method for determining the minimum embedding dimension of a scalar time series. *Physica D: Nonlinear Phenomena*, **110 (1-2)**, 43–50.

Chang, E. K., and Y. Guo, 2007: Is the number of north atlantic tropical cyclones significantly underestimated prior to the availability of satellite observations? *Geophysical Research Letters*, **34 (14)**.

Crisanti, A., M. Falcioni, A. Vulpiani, and G. Paladin, 1991: Lagrangian chaos: transport, mixing and diffusion in fluids. *La Rivista del Nuovo Cimento (1978-1999)*, **14 (12)**, 1–80.

Dijkstra, H. A., 2013: *Nonlinear climate dynamics*. Cambridge University Press.

Elsner, J. B., 2003: Tracking hurricanes. *Bulletin of the American Meteorological Society*, **84 (3)**, 353–356.

Emanuel, K., 2017: Will global warming make hurricane forecasting more difficult? *Bulletin of the American Meteorological Society*, **98 (3)**, 495–501.

Emanuel, K., and Coauthors, 2005: *Divine wind: the history and science of hurricanes*. Oxford university press.

Faranda, D., M. C. Alvarez-Castro, G. Messori, D. Rodrigues, and P. Yiou, 2019: The hammam effect or how a warm ocean enhances large scale atmospheric predictability. *Nature communications*, **10 (1)**, 1–7.

Faranda, D., V. Lembo, M. Iyer, D. Kuzzay, S. Chibbaro, F. Daviaud, and B. Dubrulle, 2018: Computation and characterization of local subfilter-scale energy transfers in atmospheric flows. *Journal of the Atmospheric Sciences*, **75 (7)**, 2175–2186.

Faranda, D., G. Messori, and P. Yiou, 2017: Dynamical proxies of north atlantic predictability and extremes. *Scientific reports*, **7**, 41 278.

Faranda, D., and S. Vaienti, 2018: Correlation dimension and phase space contraction via extreme value theory. *Chaos: An Interdisciplinary Journal of Nonlinear Science*, **28 (4)**, 041 103.

Freitas, A. C. M., J. M. Freitas, and M. Todd, 2010: Hitting time statistics and extreme value theory. *Probability Theory and Related Fields*, **147 (3-4)**, 675–710.

Ghil, M., M. D. Chekroun, and E. Simonnet, 2008: Climate dynamics and fluid mechanics: Natural variability and related uncertainties. *Physica D: Nonlinear Phenomena*, **237 (14-17)**, 2111–2126.

Grinsted, A., P. Ditlevsen, and J. H. Christensen, 2019: Normalized us hurricane damage estimates using area of total destruction, 1900- 2018. *Proceedings of the National Academy of Sciences*, **116 (48)**, 23 942–23 946.

Gualandi, A., J.-P. Avouac, S. Michel, and D. Faranda, 2020: The predictable chaos of slow earthquakes. *Science advances*, **6 (27)**, eaaz5548.

Haarsma, R. J., and Coauthors, 2016: High resolution model intercomparison project (highresmip v1. 0) for cmip6. *Geoscientific Model Development*, **9 (11)**, 4185–4208.

Hersbach, H., and Coauthors, 2020: The era5 global reanalysis. *Quarterly Journal of the Royal Meteorological Society*, **146 (730)**, 1999–2049.

Hochman, A., P. Alpert, T. Harpaz, H. Saaroni, and G. Messori, 2019: A new dynamical systems perspective on atmospheric predictability: Eastern mediterranean weather regimes as a case study. *Science advances*, **5 (6)**, eaau0936.

Kim, D., and Coauthors, 2018: Process-oriented diagnosis of tropical cyclones in high-resolution gcms. *Journal of Climate*, **31 (5)**, 1685–1702.

Klein, R., 2010: Scale-dependent models for atmospheric flows. *Annual review of fluid mechanics*, **42**, 249–274.

Knaff, J. A., C. R. Sampson, and B. R. Strahl, 2020: A tropical cyclone rapid intensification prediction aid for the joint typhoon warning center's areas of responsibility. *Weather and Forecasting*, **35 (3)**, 1173–1185.

Kossin, J., T. Hall, T. Knutson, K. Kunkel, R. Trapp, D. Waliser, and M. Wehner, 2017: Extreme storms.

Krishnamurti, T., S. Pattnaik, L. Stefanova, T. V. Kumar, B. P. Mackey, A. O'shay, and R. J. Pasch, 2005: The hurricane intensity issue. *Monthly weather review*, **133 (7)**, 1886–1912.

Landsea, C. W., and J. L. Franklin, 2013: Atlantic hurricane database uncertainty and presentation of a new database format. *Monthly Weather Review*, **141 (10)**, 3576–3592.

Latora, V., and M. Baranger, 1999: Kolmogorov-sinai entropy rate versus physical entropy. *Physical Review Letters*, **82 (3)**, 520.

Lee, C.-Y., M. K. Tippett, A. H. Sobel, and S. J. Camargo, 2016: Rapid intensification and the bimodal distribution of tropical cyclone intensity. *Nature communications*, **7 (1)**, 1–5.

Levich, E., and E. Tzvetkov, 1985: Helical inverse cascade in three-dimensional turbulence as a fundamental dominant mechanism in mesoscale atmospheric phenomena. *Physics reports*, **128 (1)**, 1–37.

Lorenz, E. N., 1963: Deterministic nonperiodic flow. *Journal of atmospheric sciences*, **20 (2)**, 130–141.

Lorenz, E. N., 1990: Can chaos and intransitivity lead to interannual variability? *Tellus A*, **42 (3)**, 378–389.

Lucarini, V., D. Faranda, and J. Wouters, 2012: Universal behaviour of extreme value statistics for selected observables of dynamical systems. *Journal of statistical physics*, **147 (1)**, 63–73.

Lucarini, V., and Coauthors, 2016: *Extremes and recurrence in dynamical systems*. John Wiley & Sons.

Messori, G., R. Caballero, and D. Faranda, 2017: A dynamical systems approach to studying midlatitude weather extremes. *Geophysical Research Letters*, **44 (7)**, 3346–3354.

Messori, G., and D. Faranda, 2021: Characterising and comparing different palaeoclimates with dynamical systems theory. *Climate of the Past*, **17 (1)**, 545–563.

Moloney, N. R., D. Faranda, and Y. Sato, 2019: An overview of the extremal index. *Chaos: An Interdisciplinary Journal of Nonlinear Science*, **29 (2)**, 022 101.

Muller, C. J., and D. M. Romps, 2018: Acceleration of tropical cyclogenesis by self-aggregation feedbacks. *Proceedings of the National Academy of Sciences*, **115 (12)**, 2930–2935.

Roberts, M. J., and Coauthors, 2020a: Impact of model resolution on tropical cyclone simulation using the highresmip–primavera multimodel ensemble. *Journal of Climate*, **33 (7)**, 2557–2583.

Roberts, M. J., and Coauthors, 2020b: Projected future changes in tropical cyclones using the cmip6 highresmip multimodel ensemble. *Geophysical Research Letters*, **47 (14)**, e2020GL088 662.

Sanders, F., 1986: Explosive cyclogenesis in the west-central north atlantic ocean, 1981–84. part i: Composite structure and mean behavior. *Monthly weather review*, **114 (10)**, 1781–1794.

Schubert, S., and V. Lucarini, 2015: Covariant lyapunov vectors of a quasi-geostrophic baroclinic model: analysis of instabilities and feedbacks. *Quarterly Journal of the Royal Meteorological Society*, **141 (693)**, 3040–3055.

Smith, A. B., and R. W. Katz, 2013: Us billion-dollar weather and climate disasters: data sources, trends, accuracy and biases. *Natural hazards*, **67 (2)**, 387–410.

Soloviev, A. V., R. Lukas, M. A. Donelan, B. K. Haus, and I. Ginis, 2017: Is the state of the air-sea interface a factor in rapid intensification and rapid decline of tropical cyclones? *Journal of Geophysical Research: Oceans*, **122 (12)**, 10 174–10 183.

Süveges, M., 2007: Likelihood estimation of the extremal index. *Extremes*, **10 (1)**, 41–55, doi: 10.1007/s10687-007-0034-2, URL https://doi.org/10.1007/s10687-007-0034-2.

van Beijeren, H., and J. Dorfman, 1995: Lyapunov exponents and kolmogorov-sinai entropy for the lorentz gas at low densities. *Physical review letters*, **74 (22)**, 4412.

Vulpiani, A., 2010: *Chaos: from simple models to complex systems*, Vol. 17. World Scientific.

Wolf, A., J. B. Swift, H. L. Swinney, and J. A. Vastano, 1985: Determining lyapunov exponents from a time series. *Physica D: Nonlinear Phenomena*, **16 (3)**, 285–317.

Young, L.-S., 1982: Dimension, entropy and lyapunov exponents. *Ergodic theory and dynamical systems*, **2 (1)**, 109–124.

Zhai, A. R., and J. H. Jiang, 2014: Dependence of us hurricane economic loss on maximum wind speed and storm size. *Environmental Research Letters*, **9 (6)**, 064 019.

LIST OF TABLES

Wilkoxon paired tests, Figure 3																
d_{SLP}	TS	HU	EX	d_{KE}	TS	HU	EX	θ_{SLP}	TS	HU	EX	θ_{KE}	TS	HU	EX
TS	–	***	***	TS	–	***	***	TS	–	***	***	TS	–	***	***
HU	–	–	n.s.	HU	–	–	***	HU	–	–	***	HU	–	–	n.s.
Wilkoxon paired tests, Figure 4																
d_{VH}	TS	HU	EX	d_W	TS	HU	EX	θ_{VH}	TS	HU	EX	θ_W	TS	HU	EX
TS	–	***	***	TS	–	***	***	TS	–	***	***	TS	–	***	***
HU	–	–	n.s.	HU	–	–	***	HU	–	–	n.s.	HU	–	–	***
Anderson-Darling paired tests, Figure 3																
d_{SLP}	TS	HU	EX	d_{KE}	TS	HU	EX	θ_{SLP}	TS	HU	EX	θ_{KE}	TS	HU	EX
TS	–	***	***	TS	–	***	***	TS	–	***	***	TS	–	***	***
HU	–	–	***	HU	–	–	***	HU	–	–	***	HU	–	–	***
Anderson-Darling paired tests, Figure 4																
d_{SLP}	TS	HU	EX	d_{KE}	TS	HU	EX	θ_{SLP}	TS	HU	EX	θ_{KE}	TS	HU	EX
TS	–	***	***	TS	–	***	***	TS	–	***	***	TS	–	***	***
HU	–	–	***	HU	–	–	***	HU	–	–	***	HU	–	–	***

TABLE 1. Summary of the results of the pairwise statistical tests. The *** symbol denotes statistical significance at the level $\alpha = 0.05$; 'n.s.' indicates non significant results. The Wilkoxon test detects pairwise location differences, the Anderson-Darling test general shape differences.

LIST OF FIGURES

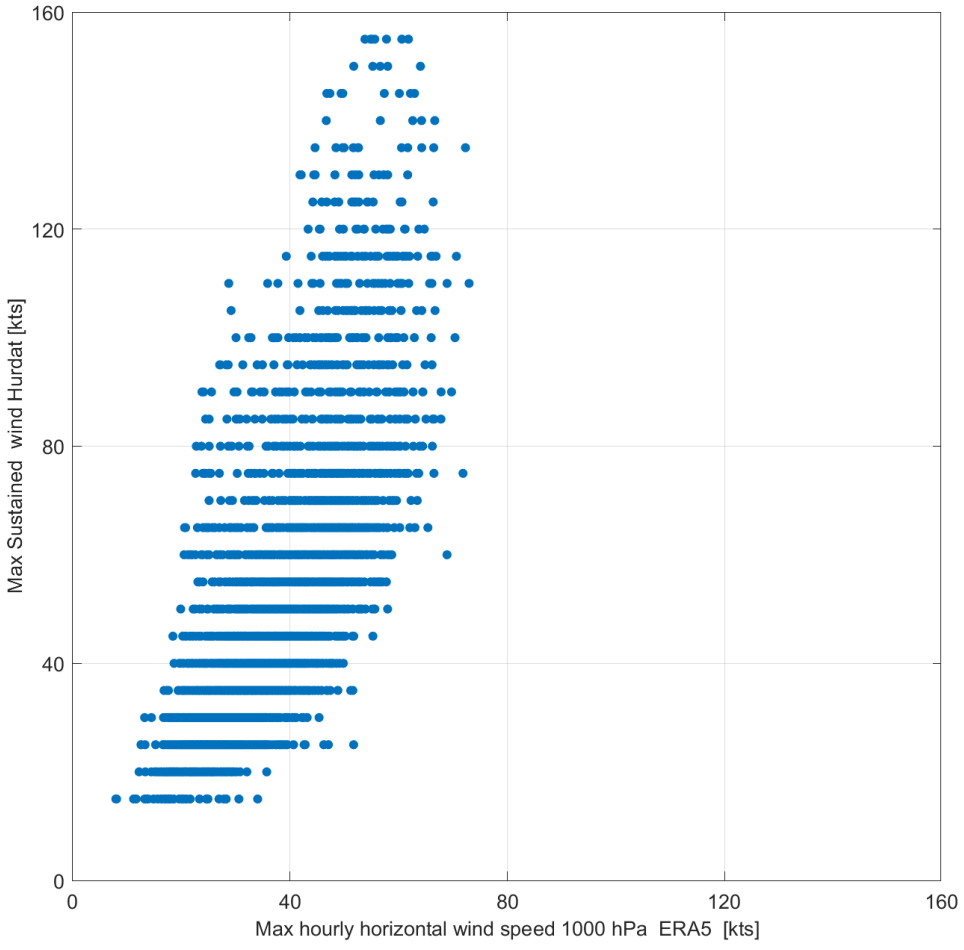

FIG. 1. Maximum horizontal hourly wind at 1000 hPa computed from the ERA5 dataset versus maximum sustained wind from the HURDAT2 database. Results are displayed in knots.

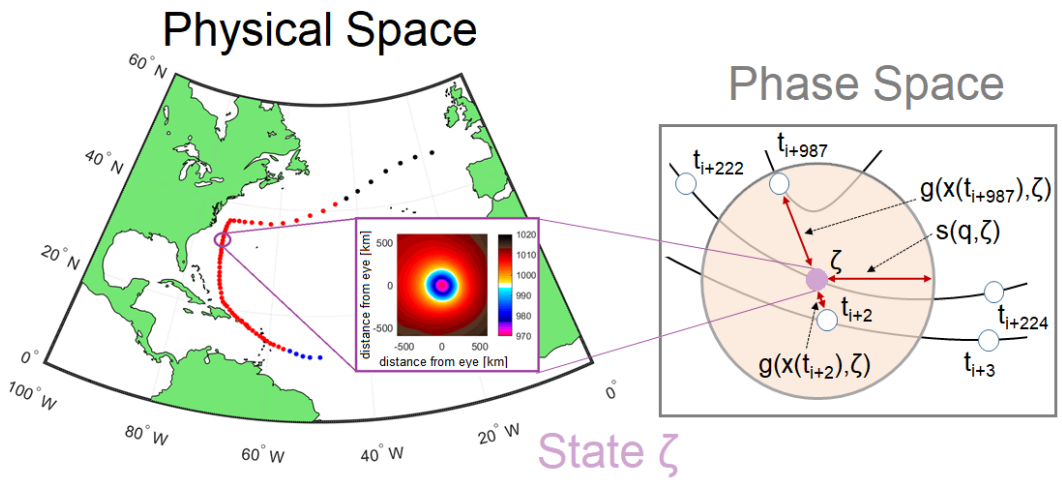

FIG. 2. Schematic of the computation of the dynamical systems metrics for an instantaneous state of a tropical cyclone. We take a snapshot of the cyclone in physical space (black quadrant), in this example a latitude-longitude map of sea-level pressure, which corresponds to state ζ in our phase space. All trajectory segments shown in the right hand side panel are part of a single, long trajectory $x(t)$, sampled at discrete times (white circles). The shaded circle is a 2D representation of the hyper-sphere determined by the high threshold $s(q,\zeta)$, which defines recurrences. The logarithmic distances between measurements defined by $g(x(t),\zeta)$ are marked by double-headed arrows. For all points within the hyper-sphere, $g(x(t),\zeta) > s(q,\zeta)$ holds. In the schematic, only two measurements satisfy this condition (adapted from (Messori and Faranda 2021)).

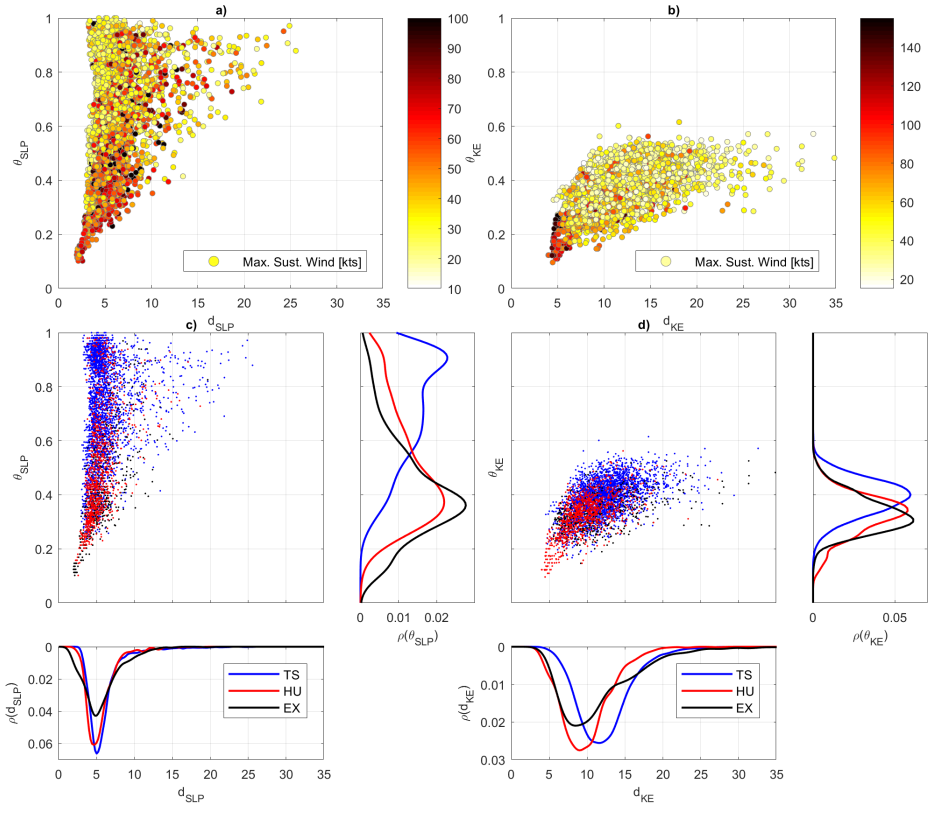

FIG. 3. Dimension d and inverse persistence θ diagrams calculated on sea-level pressure (SLP; a, c) and kinetic energy (KE; b, d). Colours show maximum sustained wind [kts] from the HURDAT2 database (a,b) and the cyclone classification (c,d, see legend). Side panels show normalized histogram counts ρ using MATLAB function *ksdensity*. TS: Tropical Storm; HU: Hurricane; EX: Extratropical transitions.

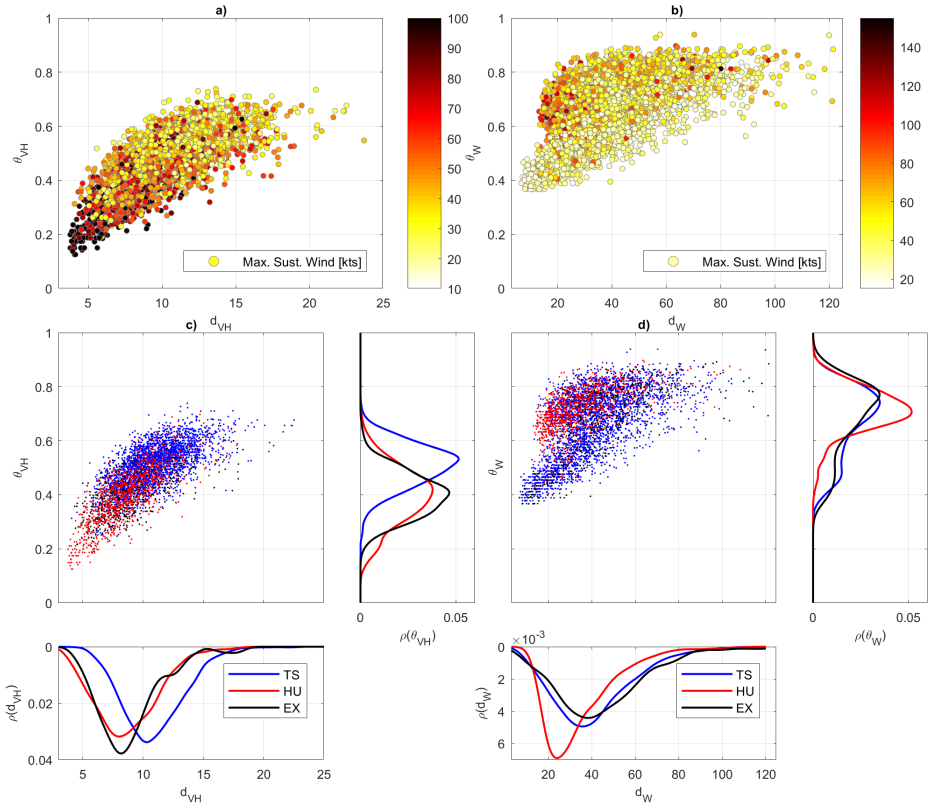

FIG. 4. Dimension d and inverse persistence θ diagrams calculated on horizontal wind at 1000hPa (VH; a, c) and vertical wind(W; b, d). Colours show maximum sustained wind [kts] from the HURDAT2 database (a,b) and the cyclone classification (c,d, see legend). Side panels show normalized histogram counts ρ using MATLAB function *ksdensity*. TS: Tropical Storm; HU: Hurricane; EX: Extratropical transitions

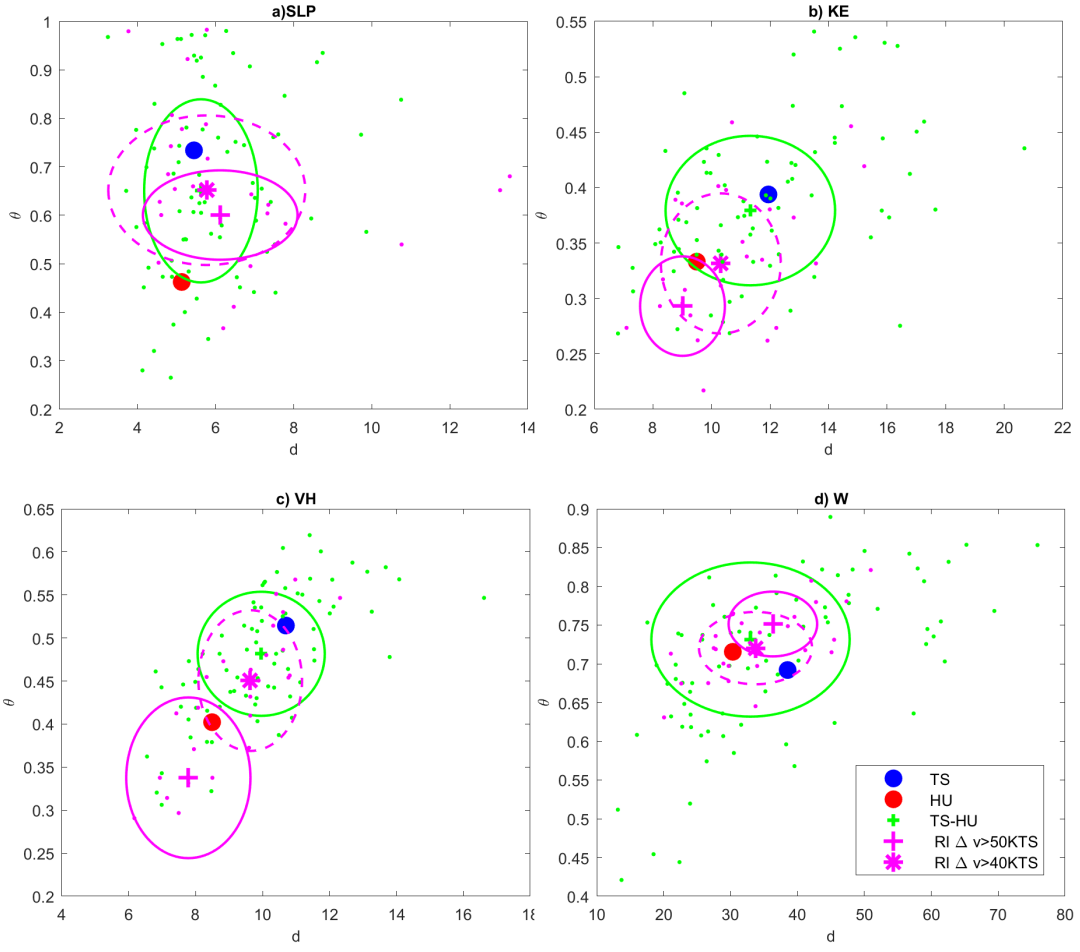

FIG. 5. Dimension d and inverse persistence θ diagrams calculated on sea-level pressure (SLP; a), kinetic energy (KE; b), horizontal wind at 1000hPa (VH; c) and vertical wind(W; d). The filled large circles indicate the median locations of Tropical Storms (blue) and Hurricanes (red), green ellipses indicate one standard deviation from the median (green crosses) of Tropical storms to Hurricanes transitions. Rapid intensification with increases in maximum sustained winds of 50 Kts (cross, solid) and 40 kTs (star, dotted) and the respective standard deviations (ellipses) are marked in purple. Single transitions are indicated as dots.